Polarization-Resolved Study of High Harmonics from Bulk Semiconductors

Keisuke Kaneshima, Yasushi Shinohara, Kengo Takeuchi, Nobuhisa Ishii, Kotaro Imasaka, Tomohiro Kaji, Satoshi Ashihara, Kenichi L. Ishikawa, and Jiro Itatani

Phys. Rev. Lett. **120**, 243903 — Published 12 June 2018

DOI: 10.1103/PhysRevLett.120.243903

Polarization-Resolved Study of High Harmonics from Bulk Semiconductors

Keisuke Kaneshima,[1,*] Yasushi Shinohara,[2,*] Kengo Takeuchi,[1] Nobuhisa Ishii,[1] Kotaro Imasaka,[3] Tomohiro Kaji,[3] Satoshi Ashihara,[3] Kenichi L. Ishikawa,[2,4] and Jiro Itatani[1]

[1] *The Institute for Solid State Physics, The University of Tokyo, 5-1-5 Kashiwanoha, Kashiwa, Chiba 277-8581, Japan*
[2] *Photon Science Center, School of Engineering, The University of Tokyo, 7-3-1 Hongo, Bunkyo-ku, Tokyo 113-8656, Japan*
[3] *Institute of Industrial Science, The University of Tokyo, 4-6-1 Komaba, Meguro-ku, Tokyo 153-8505, Japan*
[4] *Department of Nuclear Engineering and Management, School of Engineering, The University of Tokyo, 7-3-1 Hongo, Bunkyo-ku, Tokyo 113-8656, Japan*

(Dated: May 1, 2018)

The polarization property of high harmonics from gallium selenide is investigated using linearly polarized mid-infrared laser pulses. With high electric field, the perpendicular polarization component of the odd harmonics emerges, which is not present with low electric field and cannot be explained by the perturbative nonlinear optics. A two-dimensional single-band model is developed to show that anisotropic curvature of an energy band of solids, which is pronounced in an outer part of the Brillouin zone, induces the generation of the perpendicular odd harmonics. This model is validated by three-dimensional quantum mechanical simulations, which reproduce the orientation dependence of the odd-order harmonics. The quantum mechanical simulations also reveal that the odd- and even-order harmonics are produced predominantly by the intraband current and interband polarization, respectively. These experimental and theoretical demonstrations clearly show a strong link between the band structure of a solid and the polarization property of the odd-order harmonics.

PACS numbers: 42.50.Hz, 42.65.Ky, 72.20.Ht, 42.65.-k

High harmonic generation (HHG) in gaseous media is a universal phenomenon that reflects extreme nonlinear interactions between a strong electric field and bound and/or unbound electrons of atoms and molecules. The constitutional three steps, *i.e.*, tunneling ionization, electron acceleration, and recombination are well understood [1], which leads to a novel spectroscopic method called high harmonic spectroscopy. This powerful tool has become indispensable in attosecond physics to probe the electron dynamics and to reconstruct orbital structures with attosecond and ångström resolutions [2, 3].

Recently, high harmonic radiation beyond the bandgap energy has been produced in crystalline solids [4–7]. Solid HHG is distinctively different from gas HHG in two aspects. First, there exist two sources of HHG radiation: intraband current in a band and interband polarization between two bands. Role of the intraband current and interband polarization has been studied experimentally and theoretically [4, 6–12]. However, a physical picture of the radiation mechanism is not fully established yet. Second, crystallographic orientation with respect to the polarization direction of a drive laser field strongly influences the generation of high harmonics [4, 6, 9, 13], which results from field-driven electron dynamics in a periodic structure. Therefore, solid HHG is becoming a spectroscopic method that allows to access the band structure of solids [7, 14]. However, most of solid HHG experiments use one-dimensional (1D) analysis. Although a 1D picture is simple and intuitive, it cannot fully describe the extremely nonlinear light-matter interaction because of the three-dimensional (3D) structure of solids and the vector nature of electric fields. Therefore, multidimensional analysis is indispensable in high harmonic spectroscopy of solids.

Recently, ellipticity in drive lasers has been introduced to enhance and/or

diminish the harmonic yield [15, 16] as well as to investigate selection rules [17–19]. Polarization analyses of high harmonics have been demonstrated [20, 21], however, both works mainly focus on even harmonics. F. Langer *et al.* treat multi-dimensional problems by a linear combination of a 1D Bloch equation [21]. H. Liu *et al.*, introduce the Berry curvature to a single-band model to explain perpendicularly polarized even harmonics [20].

In this study, we investigate a polarization property of odd-order high harmonics produced from a semiconductor gallium selenide (GaSe) crystal exposed to femtosecond mid-infrared (MIR) pulses and their dependence on crystallographic orientation. With high electric field applied, the perpendicularly polarized components of the odd harmonics emerge with a counter-intuitive 30° periodicity. A two-dimensional (2D) single-band model successfully explains that anisotropic curvature of an energy band of solids induces the perpendicular intraband current, resulting in the emergence of the perpendicularly polarized odd harmonics. This 2D single-band model is

* These authors contributed equally to this work

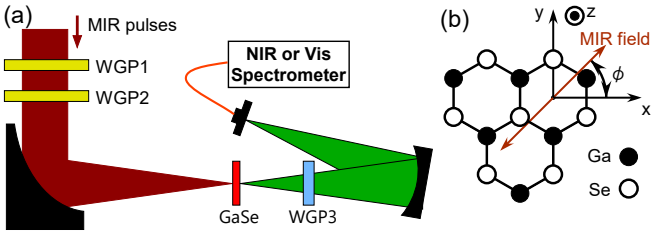

FIG. 1. Polarization-resolved measurement of high harmonics from GaSe. (a) Experimental setup: WGP1, WGP2, and WGP3, wire-grid polarizers; GaSe, 30-μm-thick gallium selenide crystal. (b) Top view of the GaSe lattice structure and the definition of the orientation angle, ϕ.

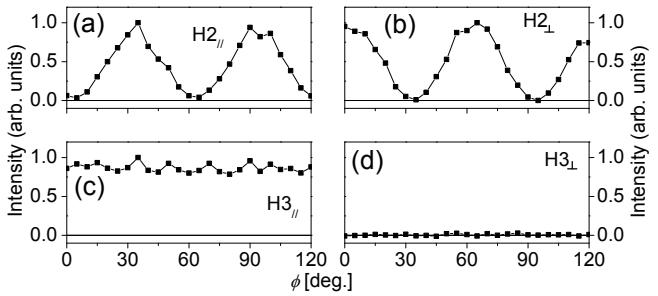

FIG. 2. Rotation angle dependence with a low electric field of 3.2 MV/cm. Curve plots for the parallel second (a), perpendicular second (b), parallel third (c), and perpendicular third (d) harmonics.

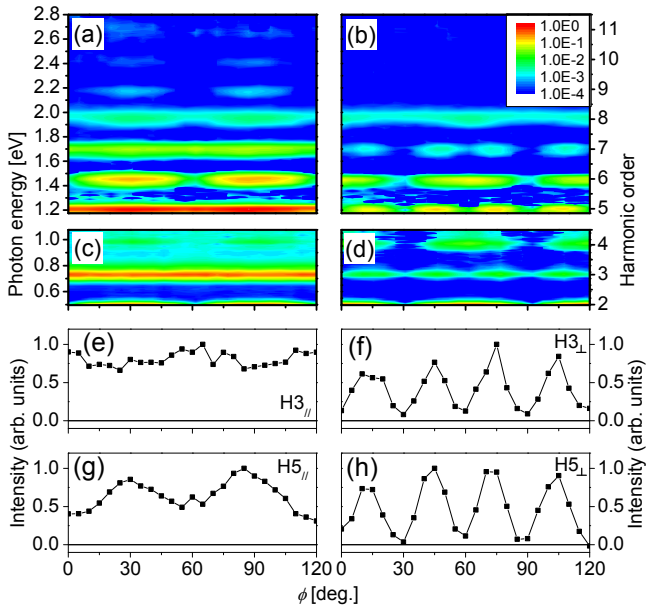

FIG. 3. Rotation angle dependence with a high field amplitude of 10 MV/cm. The parallel (a, VIS; c, IR) and perpendicular (b, VIS; d, IR) polarization components of the high harmonics as a function of the rotation angle. Curve plots of the parallel third (e), perpendicular third (f), parallel fifth (g), and perpendicular fifth (h) harmonics.

validated by 3D *ab-initio* time-dependent density matrix (TDDM) simulations. The TDDM simulations well reproduce the experimental orientation dependence and reveal that the odd- and even-order harmonics are produced predominantly by the intraband current and interband polarization, respectively.

A 30-μm-thick GaSe crystal (non-coat, z-cut, ε-type) is irradiated by linearly polarized MIR pulses (5 μm, 15 μJ, 200 fs, 1 kHz) [22]. Detail of our infrared light source is described in the supplement. As shown in Fig. 1(a), two wire-grid polarizers control the pulse energy and linearize the MIR field. The MIR beam is focused ($f = 100$ mm) down to a measured size of 64 μm (full width at $1/e^2$ intensity),

resulting in a peak amplitude of 33.7 MV/cm in the air. The GaSe crystal is mounted at normal incidence to allow rotation along its z axis. GaSe is a uniaxial hexagonal crystal (Fig. 1(b)), and has a graphite-type structure with a four-fold (Se-Ga-Ga-Se) layer. An ε-type GaSe belongs to the $\bar{6}$m2 (D_{3h}) symmetry point group. The bandgap energy is 1.98 eV (625 nm in wavelength) at room temperature and the transparency range extends from 0.65 to 18 μm [23]. An analyzing wire-grid polarizer selects the polarization of the high harmonics. The spectrum of the high harmonics is measured both in the near-infrared (NIR) (NIRQuest256-2.5, Ocean Optics) and the visible (VIS) (USB4000-XR, Ocean Optics) regions. The dependence of HHG on the rotation angle ϕ, which is defined as in Fig. 1(b), is measured with two electric field amplitudes. With a lower electric field of 3.2 MV/cm in the crystal, we observe the second and third harmonics. The second harmonic polarized parallel to the MIR field (Fig. 2(a)) is maximized at $\phi = 30° + 60° \times n$ with n being an integer, *i.e.*, when the input field is applied along the Ga-Se bond direction (see Fig. 1(b)). Meanwhile, the perpendicularly polarized second harmonic (Fig. 2(b)) is maximized at $\phi = 60° \times n$. This observation is consistent with a preceding work [6] and

can be explained by the hexagonal structure of a GaSe crystal. Indeed, these orientation dependences agree quantitatively well with $\sin^2 3\phi$ and $\cos^2 3\phi$ for the parallel and perpendicular harmonics, respectively, which are calculated by using the second-order susceptibility tensor [24].

The parallel component of the third harmonic (Fig. 2(c)) is found to be constant regardless of the orientation, while a perpendicular component (Fig. 2(d)) are virtually absent. These results are also consistent with the angle dependences calculated by the third-order nonlinear tensors [25], which are constant and zero for the parallel and perpendicular polarization components, respectively. Thus, with this low field, the orientation dependences of all harmonics are

well explained by the perturbative nonlinear optics.

With a higher electric field of 10 MV/cm in the crystal, we measure the orientation dependences of the parallel (Figs. 3(a), VIS; (c), IR) and perpendicular (Figs.

3(b), VIS; (d), IR) high harmonics. The high harmonics extend up to the eleventh order (2.70 eV, 460 nm) beyond the band gap (1.98 eV, 625 nm). The eighth harmonic signals around 1.95 eV are overlapped with isotropic interband photoluminescence. All even harmonics for both polarizations show modulations with 60° periodicities similar to the second harmonics with the lower electric field. On the other hand, in contrast to the low intensity case, the *parallel odd* harmonics show 60° periodicity as in Figs. 3(e) and (g) for the third and fifth harmonics respectively. Even more surprisingly, the *perpendicular odd* harmonics appear with 30° periodicity as in Figs. 3(f) and (h) for the third and fifth harmonics, respectively. These observations cannot be explained by the third-order nonlinearity, suggesting the onset of a non-perturbative response. In particular, the 30° periodicity in the perpendicular third harmonic cannot be intuitively understood from the hexagonal structure of the crystal.

To explain the experimental results, a 2D single-band model described by the Bloch theorem is used. In a 1D case, similar models have been frequently used [4, 6, 26]. This model assumes that (i) the intraband current dominates the odd harmonics and (ii) the electron wavepacket is launched around the Γ point, both of which have been verified by the TDDM simulations. The dominance of the intraband current for odd harmonics in GaSe is also experimentally verified [6]. Γ point

The momentum of an electron wavepacket $\boldsymbol{k}(t)$ ($\boldsymbol{k}(0) = 0$) with charge, $-e$, is described by the acceleration theorem in the presence of an oscillating electric field $\boldsymbol{E}_{\rm L}(t)$ as $\frac{d}{dt}\boldsymbol{k}(t) = -\frac{e}{\hbar}\boldsymbol{E}_{\rm L}(t)$. The macroscopic intraband current $\boldsymbol{J}(t)$ is related to the group velocity $\boldsymbol{v}_{\boldsymbol{k}} = \frac{1}{\hbar}\frac{dE_{\boldsymbol{k}}}{d\boldsymbol{k}}$ of the electron wavepacket integrated over the first Brillouin zone with $E_{\boldsymbol{k}}$ being the band energy as

$$\boldsymbol{J}(t) = -\int_{\rm BZ} e\boldsymbol{v}_{\boldsymbol{k}} n_{\boldsymbol{k}}(t) d\boldsymbol{k} = -\frac{e}{\hbar}\left.\frac{dE_{\boldsymbol{k}}}{d\boldsymbol{k}}\right|_{\boldsymbol{k}=\boldsymbol{k}(t)}. \quad (1)$$

Here, the initial wavepacket is assumed to be localized at the Γ point without spread by setting the electron density as $n_{\boldsymbol{k}}(t) = \delta(\boldsymbol{k} - \boldsymbol{k}(t))$. The induced electric field $\boldsymbol{E}^{\rm HH}(t)$ generated by the intraband current is obtained as,

$$\boldsymbol{E}^{\rm HH}(t) \propto \frac{d\boldsymbol{J}(t)}{dt} = \frac{e^2}{\hbar^2}\frac{d^2E_{\boldsymbol{k}}}{d\boldsymbol{k}^2}\boldsymbol{E}_{\rm L}(t) \propto \left(\frac{1}{m^*_{\boldsymbol{k}}}\right)\boldsymbol{E}_{\rm L}(t), \quad (2)$$

where $\frac{d^2E_{\boldsymbol{k}}}{d\boldsymbol{k}^2}$ and $\frac{1}{m^*_{\boldsymbol{k}}}$ are the band curvature and the inverse effective mass, respectively, both of which are rank two tensors and can be represented by a 2 x 2 matrix in the xy plane. The input and induced electric fields are decomposed in the parallel and perpendicular directions as $\boldsymbol{E}_{\rm L}(t) = (E_{\rm L}(t), 0)$ and $\boldsymbol{E}^{\rm HH}(t) = \left(E^{\rm HH}_{\parallel}(t), E^{\rm HH}_{\perp}(t)\right)$, respectively. By using the band curvature tensor, the induced field components are explicitly written as $E^{\rm HH}_{\parallel}(t) \propto \frac{\partial^2 E_{\boldsymbol{k}}}{\partial k^2_{\parallel}}\left(\equiv E_{k_\parallel k_\parallel}\right) \times E_{\rm L}(t)$ and $E^{\rm HH}_{\perp}(t) \propto \frac{\partial^2 E_{\boldsymbol{k}}}{\partial k_{\parallel}\partial k_{\perp}}\left(\equiv E_{k_\parallel k_\perp}\right) \times E_{\rm L}(t)$, showing that the band curvature is the source of an induced radiation. The momentum dependence of the band curvature along the electron trajectory is the source of odd-order harmonics, while the constant term of the curvature is responsible for the linear response. Figures 4(a), (b), and (c) represent the lowest conduction band calculated by the density-functional theory (DFT) and its curvatures $E_{k_\parallel k_\parallel}$ and $E_{k_\parallel k_\perp}$, respectively. In these figures, we illustrate three electron trajectories at $\phi = 60°$ (solid black arrows), 45° (dash), and 30° (dot) and the maximum amplitudes of electron transportation with electric fields of 3.2 (dashed black circles) and 10 MV/cm (solid black circles). Figure 4(c) reveals that any perpendicular harmonic is not produced with a low electric field, because $E_{k_\parallel k_\perp}$ is nearly zero around the Γ point. This is consistent with the experimental results with the 3.2-MV/cm electric field. On the other hand, with a high electric field, the per-

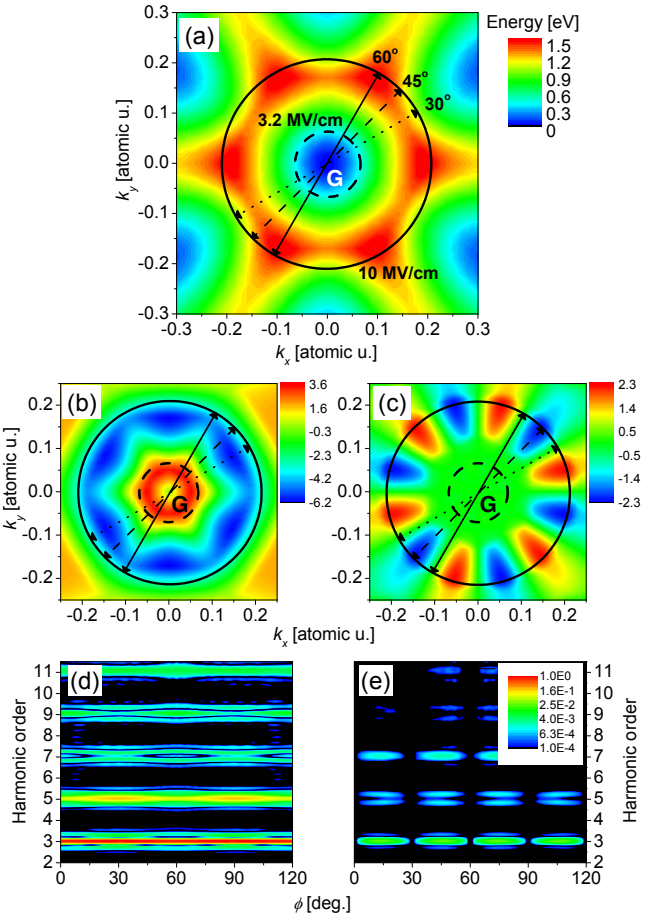

FIG. 4. (a) Lowest conduction band of GaSe and its band curvatures (b) $E_{k_\parallel k_\parallel}$ and (c) $E_{k_\parallel k_\perp}$. Three electron trajectories at $\phi = 60°$ (solid black arrows), 45° (dash), and 30° (dot) are illustrated. The maximum amplitudes of electron trajectories with electric fields of 3.2 and 10 MV/cm are shown by the dashed and solid black circles, respectively. Orientation dependence of the (d) parallel and (e) perpendicular harmonics obtained by the 2D single-band model with the 10-MV/cm electric field.

pendicular harmonics can be generated, because $E_{k_\parallel k_\perp}$ becomes non-zero in an outer momentum area ($|\boldsymbol{k}| > 0.1$ atomic unit) except orientation angles of $\phi = 30° \times n$. This explanation is consistent with the orientation dependences of the perpendicular odd harmonics obtained with the 10 MV/cm electric field. Regarding the parallel odd harmonics, $E_{k_\parallel k_\parallel}$ in Fig. 4(b) is isotropic around the Γ point and shows 60° periodicities in an outer part. This consideration is also consistent with the experimental results for the parallel odd harmonics. Based on this 2D single-band model, the parallel and perpendicular odd harmonics are calculated to show the 60° and 30° periodicities as in Fig. 4(d) and (e), respectively. These results well reproduce the experimental observations of the orientation dependences and the polarization property for all odd harmonics. It should be noticed that the single-band model cannot explain the generation of even harmonics, since the band structure in Fig. 4(a) has an inversion symmetry. $30° \times n$, ionQuantum-mechanical simulation

To understand the extreme nonlinear response of the unit cell of GaSe exposed to an electric field, we develop an independent-particle TDDM model combined with the band information obtained by DFT. This 3D *ab-initio* quantum mechanical model performs simulation on HHG from GaSe irradiated by a laser pulse (4.96 μm, 104 fs, 10.0 MV/cm) similar to those used in the experiment. This simulation includes 103 bands spanning 39 eV in energy, of which 38 bands are initially occupied as valence bands. HHG spectra are obtained by the Fourier transform of the induced current including both intraband and interband contributions, which can also be evaluated separately by using the projection onto instantaneous eigenfunctions as discussed later. The simulation are described in detail in the supplement.

In Fig. 5, the parallel (a) and perpendicular (b) components of the odd and even order harmonics are plotted as a function of the rotation angle. For all perpendicular odd harmonics, this simulation result clearly reproduces the 30° periodicity of the experimental observation as shown in Figs. 5(b), (d), and (f). Similarly, the 60° periodicity of the parallel odd harmonics is present, as in Figs. 5(a), (c), and (e). Regarding the even harmonics, the simulation reproduces the 60° periodicities for the parallel and perpendicular components with a relative orientation shift of 30°, which is also consistent with the experimental results. Although the bulk response is well described, there is a difficulty in quantitative comparison with the experimental results due to the neglect of relaxation[14] and light-field propagation[27].

and

Intraband current and interband polarization HHG in solids has two sources of radiation: intraband current and interband polarization. The TDDM simulation can disentangle these two terms. In Figs. 6(a) and (b), the shaded areas represent the simulated spectra of the parallel and perpendicular harmonics at $\phi = 15°$, respectively. The red and blue curves show the contributions from

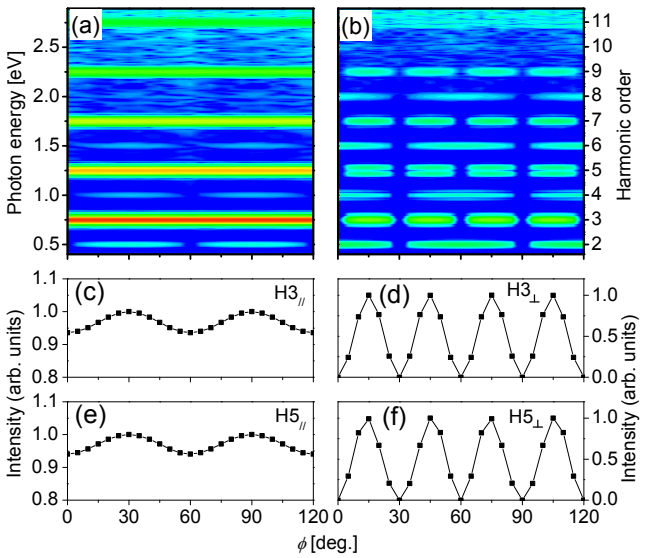

FIG. 5. Simulated rotation angle dependence of the high harmonics with a field amplitude of 10.0 MV/cm. Orientation-dependent spectra of the parallel (a) and perpendicular (b) harmonics. Line plots of the parallel third (c), perpendicular third (d), parallel fifth (e), and perpendicular fifth (f) harmonics.

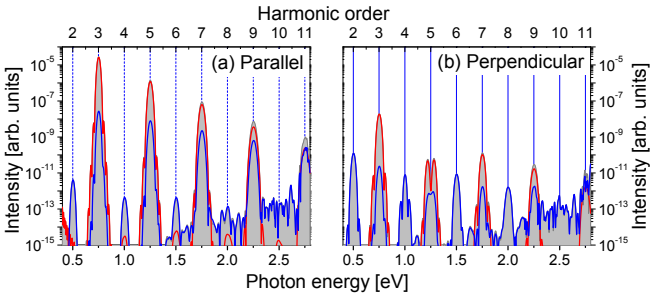

FIG. 6. Simulated contributions of the intraband current and interband polarization. (a) High harmonic spectrum of the parallel components (shaded area) at $\phi = 15°$ and its decomposition into the intraband current (red curve) and the interband polarization (blue curve). (b) the same plot as (a) for the perpendicular components.

the intraband current and the interband polarization, respectively. In both polarizations, the odd harmonics are predominantly produced by the intraband current. At higher orders, especially above the band gap, the contribution of the interband polarization catches up with that of the intraband current. On the other hand, the interband contribution dominates all even harmonics regardless of the polarization state. This clear decomposition of the radiation source is checked to be valid at other orientation angles. This is the first demonstration of the explicit decomposition.

system has

In summary, we have investigated a polarization property of the high harmonics from a GaSe bulk crystal using

femtosecond MIR pulses and their dependence on crystallographic orientation. The experimental results with the 3.2 MV/cm electric field are well explained by the perturbative nonlinear optics. In contrast, with the 10 MV/cm electric field, the perpendicular odd harmonics emerges with a periodic modulation of 30°, which cannot be explained by the perturbative nonlinear optics. The physical origin of the perpendicular component of the odd harmonics is attributed to anisotropic momentum dependence of the band curvature along the electron trajectory, which is equivalent to the inverse effective mass.

We perform 3D *ab-initio* TDDM simulations, which qualitatively reproduce the experimental observation and reveals that the even and odd harmonics are dominantly produced by the interband polarization and the intraband current, respectively. Our demonstration establishes a direct link between the band structure of a solid and HHG in a solid. Multi-dimensional analysis combined with time-resolved measurement allows to investigate electron dynamics and field-dressed structure of energy bands. ,Gaarde2

We acknowledge support from JSPS KAKENHI (Grant numbers: 23226003, 25286064, 25790063, 26390076, 26600111, 15K13375, 16H03881, and 17H04816). Quantum Basic Research Coordinated Development Program, the Photon Frontier Network Program, and "Exploratory Challenge on Post-K computer" from MEXT as well as the Center of Innovation (COI) Program and Core Research for Evolutional Science and Technology (CREST) (Grant number: JPMJCR15N1) from the Japan Science and Technology Agency (JST). K. K. is supported by Program for Leading Graduate Schools (MERIT) by Japan Society for the Promotion of Science. The computation in this work has been done using the facilities of the Supercomputer Center, the Institute for Solid State Physics, the University of Tokyo. This research also used computational resources of the K computer provided by the RIKEN Advanced Institute for Computational Science through the HPCI System Research project (Project ID: hp160260). We thank Professors Takeo Kato, Koichiro Tanaka, and Hidefumi Akiyama for enlightening discussions.

[1] P. B. Corkum, Phys. Rev. Lett. **71**, 1994 (1993).
[2] P. B. Corkum and F. Krausz, Nature Physics **3**, 381 (2007).
[3] J. Itatani, J. Levesque, D. Zeidler, H. Niikura, H. Pépin, J. C. Kieffer, P. B. Corkum, and D. M. Villeneuve, Nature **432**, 867 (2004).
[4] S. Ghimire, A. D. DiChiara, E. Sistrunk, P. Agostini, L. F. DiMauro, and D. A. Reis, Nature Physics **7**, 138 (2011).
[5] F. Krausz and M. I. Stockman, Nature Photonics **8**, 205 (2014).
[6] O. Schubert, M. Hohenleutner, F. Langer, B. Urbanek, C. Lange, U. Huttner, D. Golde, T. Meier, M. Kira, S. W. Koch, and R. Huber, Nature Photonics **8**, 119 (2014).
[7] T. T. Luu, M. Garg, S. Y. Kruchinin, A. Moulet, M. T. Hassan, and E. Goulielmakis, Nature **521**, 498 (2015).
[8] G. Vampa, T. J. Hammond, N. Thiré, B. E. Schmidt, F. Légaré, C. R. McDonald, T. Brabec, and P. B. Corkum, Nature **522**, 462 (2015).
[9] F. Langer, M. Hohenleutner, C. P. Schmid, C. Poellmann, P. Nagler, T. Korn, C. Schüller, M. S. Sherwin, U. Huttner, J. T. Steiner, S. W. Koch, M. Kira, and R. Huber, Nature **533**, 225 (2016).
[10] M. Garg, M. Zhan, T. T. Luu, H. Lakhotia, T. Klostermann, A. Guggenmos, and E. Goulielmakis, Nature **538**, 359 (2016).
[11] T. Ikemachi, Y. Shinohara, T. Sato, J. Yumoto, M. Kuwata-Gonokami, and K. L. Ishikawa, Phys. Rev. A **95**, 043416 (2017).
[12] T. Ikemachi, Y. Shinohara, T. Sato, J. Yumoto, M. Kuwata-Gonokami, and K. L. Ishikawa, arXiv:1709.08153 [physics.optics].
[13] M. Wu, Y. You, S. Ghimire, D. A. Reis, D. A. Browne, K. J. Schafer, and M. B. Gaarde, Phys. Rev. A **96**, 063412 (2017).
[14] G. Vampa, T. J. Hammond, N. Thiré, B. E. Schmidt, F. Légaré, C. R. McDonald, T. Brabec, D. D. Klug, and P. B. Corkum, Phys. Rev. Lett. **115**, 193603 (2015).
[15] Y. S. You, D. A. Reis, and S. Ghimire, Nature Physics **13**, 345 (2017).
[16] N. Yoshikawa, T. Tamaya, and K. Tanaka, Science **356**, 736 (2017).
[17] N. Tancogne-Dejean, O. D. Mücke, F. X. Kärtner, and A. Rubio, Phys. Rev. Lett. **118**, 087403 (2017).
[18] N. Tancogne-Dejean, O. D. Mücke, F. X. Kärtner, and A. Rubio, Nature Communications **8**, 745 (2017).
[19] N. Saito, P. Xia, F. Lu, T. Kanai, J. Itatani, and N. Ishii, Optica **4**, 1333 (2017).
[20] H. Liu, Y. Li, Y. S. You, S. Ghimire, T. F. Heinz, and D. A. Reis, Nature Physics **13**, 262 (2017).
[21] F. Langer, M. Hohenleutner, U. Huttner, S. W. Koch, M. Kira, and R. Huber, Nature Photonics **11**, 227 (2017).
[22] K. Kaneshima, N. Ishii, K. Takeuchi, and J. Itatani, Opt. Express **24**, 8660 (2016).
[23] N. Fernelius, Prog. Crystal Growth and Charact. **28**, 275 (1994).
[24] A. Yariv, *Quantum Electronics* (John Wiley & Sons, 1988).
[25] P. S. Banks, M. D. Feit, and M. D. Perry, J. Opt. Soc. Am. B **19**, 102 (2002).
[26] O. D. Mücke, Phys. Rev. B **84(R)**, 081202 (2011).
[27] I. Floss, C. Lemell, G. Wachter, V. Smejkal, S. A. Sato, X.-M. Tong, K. Yabana, and J. Burgdörfer, Phys. Rev. A **97**, 011401(R) (2018).
[28] See Supplemental Material [url] for details of the MIR light source and TDDM simulation, which includes Refs. [29-37].
[29] M. Lindberg and S. Koch, Phys. Rev. B **38**, 3342 (1988).
[30] http://elk.sourceforge.net/.
[31] Z. H. Levine and D. C. Allan, Phys. Rev. Lett. **63**, 1719

(1989).
[32] D. Xiao, M.-C. Chang, and Q. Niu, Rev. Mod. Phys. **82**, 1959 (2010).
[33] W. Jie, X. Chen, D. Li, L. Xie, Y. Y. Hui, S. P. Lau, X. Cui, and J. Hao, Angew. Chem. Int. Ed. Engl. **54**, 1185 (2015).
[34] L. Karvonen, A. Säynätjoki, S. Mehravar, R. D. Rodoriguez, S. Hartmann, D. R. T. Zahn, S. Honkanen, R. A. Norwood, N. Peyghambarian, K. Kieu, H. Lipsanen, and J. Riikonen, Scientific Reports **5**, 10334 (2015).
[35] S. A. Sato and K. Yabana, Phys. Rev. B **89**, 224305 (2014).
[36] V. S. Yakovlev and M. S. Wismer, Computer Physics Communications **217**, 82 (2017).
[37] M. Wu, S. Ghimire, D. A. Reis, K. J. Schafer, and M. B. Gaarde, Phys. Rev. A **91**, 043839 (2015).